



Urban flux measurements reveal a large pool of oxygenated volatile organic compound emissions

T. Karl^{a,1}, M. Striednig^a, M. Graus^a, A. Hammerle^b, and G. Wohlfahrt^b

^aInstitute of Atmospheric and Cryospheric Sciences, University of Innsbruck, 6020 Innsbruck, Austria; and ^bInstitute of Ecology, University of Innsbruck, 6020 Innsbruck, Austria

Edited by Guy Brasseur, Max Planck Institute of Meteorology, Hamburg, Germany, and accepted by Editorial Board Member A. R. Ravishankara December 12, 2017 (received for review August 21, 2017)

Atmospheric chemistry is fueled by a large annual influx of non-methane volatile organic compounds (NMVOC). These compounds influence ozone formation, lead to secondary organic aerosol production, and play a significant role for the oxidizing capacity of the atmosphere. The anthropogenic NMVOC budget is considerably uncertain due to the diversity of urban emission sources. Here, we present comprehensive observations of urban NMVOC eddy covariance fluxes using a newly designed proton-transfer-reaction quadrupole interface time-of-flight mass spectrometer. We found emission fluxes of a surprisingly large pool of oxygenated NMVOCs (OVOCs) with an appreciable fraction of higher oxidized OVOCs that cannot be explained by known fast photochemical turnaround or current primary emission estimates. Measured OVOC/NMVOC bulk flux ratios are two to four times higher than inferred from aggregated anthropogenic emission inventories. Extrapolating these results would double the global anthropogenic NMVOC flux. In view of globally accelerating urbanization, our study highlights the need to reevaluate the influence of anthropogenic NMVOC on atmospheric chemistry, human health, and the climate system.

NMVOC | eddy covariance | urban emissions | air pollution | mass spectrometry

There is compelling evidence that oxygenated nonmethane volatile organic compounds (OVOC) released into the atmosphere profoundly influence oxidative processes (1–3), including the formation of secondary organic aerosols (SOA) (4–6). Urban photochemical smog has been identified as particularly diverse in ozone- and SOA-forming nonmethane volatile organic compounds (NMVOC) (7–9), but predictions of associated emissions are highly uncertain. Urban areas are generally considered NMVOC-sensitive with respect to ozone production (7, 10–12), and air quality control legislation devises measures to limit the emitted OH reactivity of the anthropogenic precursor pool (13). Comparisons between modeled and measured OH reactivity suggest significant discrepancies across different photochemical regimes, including urban areas (3, 9, 14). It is assumed that urban environments in Western economies have seen a significant transformation in the composition of NMVOC emissions fueling atmospheric chemistry during recent years. Decreasing trends in concentrations of aliphatic and aromatic compounds (11, 15, 16) have largely been attributed to decreasing emissions from automobiles since the introduction of catalytic converter technology. In addition, new pollution directives (17) have mandated a gradual manufacturing shift toward oxygenated solvents. Despite reasonably good knowledge on relative concentration trends of aliphatic and aromatic compounds, the verification of absolute emissions of anthropogenic NMVOC databases remains difficult (18, 19) because the anthropogenic budget of OVOC has been identified as particularly uncertain (7, 20). Consequently, the global emission flux of anthropogenic NMVOC is quite uncertain. While oxygenated compounds are often considered less toxic and rank lower on the ozone reactivity scale (13), their influence on SOA formation is considered important due to their high solubilities and low vapor pressures (21). This has consequences for a quantitative

understanding of climate feedbacks as SOA can efficiently alter cloud formation processes. An increased presence of oxygenated compounds can also potentially present an emerging challenge for air pollution management as SOA is an acute public health concern in many regions. Here we show that a surprisingly large proportion of multifunctional oxygenated NMVOC is injected into the lower atmosphere which cannot be explained by known photochemical production or inferred from bottom-up emission inventories.

Results

Measurements were performed with a newly designed proton-transfer-reaction time-of-flight mass spectrometer with quadrupole interface (PTR-QiTOF) (*Methods*) using the eddy covariance (EC) method. The instrument's performance allowed a 10-fold decrease in flux detection limits compared with previous studies. It was therefore possible to quantify a significantly larger number of individual NMVOC fluxes by this technique than in the past. Soft chemical ionization based on proton-transfer reactions (PTR) has proven a valuable method for EC measurements of NMVOC (22, 23) requiring the detection of ultrafast concentration fluctuations (e.g., 10 Hz and higher) in combination with minimal sampling losses. The EC method is fundamentally derived from the scalar budget equation after Reynolds decomposition, and in its simplest form for horizontally homogeneous flows normal to the surface, where the mean vertical motion of wind (\bar{w}) can be considered zero, relates the measured

Significance

The exchange of nonmethane volatile organic compounds (NMVOC) at the surface–atmosphere interface is a fundamental constraint and important boundary condition for atmospheric chemistry and its effects on climate. Anthropogenic emissions are thought to account for about half of the NMVOC flux into the atmosphere of the Northern Hemisphere, yet their budget is considerably uncertain due to the scarcity of appropriate top-down constraints. Here we present direct flux measurements of NMVOCs based on the eddy covariance technique, showing that the contribution of typical urban emission sources is comprised of a surprisingly large portion of oxygenated NMVOC. These results suggest that typical urban NMVOC emission sources could be significantly higher than currently projected in air chemistry and climate models.

Author contributions: T.K. designed research; T.K., M.S., M.G., A.H., and G.W. performed research; T.K., M.S., M.G., A.H., and G.W. analyzed data; and T.K., M.G., A.H., and G.W. wrote the paper.

The authors declare no conflict of interest.

This article is a PNAS Direct Submission. G.B. is a guest editor invited by the Editorial Board.

This open access article is distributed under [Creative Commons Attribution-NonCommercial-NoDerivatives License 4.0 \(CC BY-NC-ND\)](https://creativecommons.org/licenses/by-nc-nd/4.0/).

¹To whom correspondence should be addressed. Email: thomas.karl@uibk.ac.at.

This article contains supporting information online at www.pnas.org/lookup/suppl/doi:10.1073/pnas.1714715115/-DCSupplemental.

surface–atmosphere exchange flux (F) to the covariance between vertical wind and concentration fluctuation according to

$$F = \langle w'c' \rangle, \quad [1]$$

where w' represents the vertical fluctuation of wind speed and c' the concentration fluctuation. Brackets denote the averaging interval, where a 30-min ensemble average is commonly used for atmosphere–surface exchange measurements (*Methods*). With few exceptions, proton affinities of OVOC are generally much higher than that of water, so that their detection by PTR can theoretically provide a quantitative top-down constraint of volatile oxygenates in the atmosphere measured by EC. Fig. 1 gives an overview of results for NMVOC fluxes obtained in an urban setting in central Europe during a 2-mo-long campaign during summer. The flux data were prefiltered according to standard quality assurance procedures recommended for EC measurements (*Methods*) and represent median net emission fluxes. The Kendrick mass defect plot (Fig. 1A) shows all isobaric compounds (without isotopes) in the lower mass range that yielded emission fluxes. While surface–atmosphere flux observations typically have to be interpreted as a net flux balanced between emission (upward) and deposition (downward), the absence of any significant NMVOC net deposition fluxes during this study suggests that dry deposition over urban surfaces is very limited, in contrast to vegetated surfaces (23–25). These findings support the idea that dry deposition of NMVOC over urban nonvegetated surfaces can be considered small. The degree of oxygenation and the relative abundance of oxygenated compounds exhibiting an emission flux are depicted in Fig. 1B and C, where the data are binned according to the nominal protonated mass and

the number of calculated oxygen atoms. The molar flux of oxygenates being actively emitted into the urban atmosphere inferred from this dataset is $56 \pm 10\%$ relative to the total NMVOC flux. The overall percentage of the number of oxygenated isomers detected by PTR yielding an upward flux is 74%. The heaviest volatile molecules that were still observed with an upward flux also contained the highest number of oxygen atoms (up to seven) and were tentatively identified as D3–D7 siloxanes (e.g., D5: $C_9H_{26}O_5Si_5$). Siloxanes have recently been reported as characteristic urban tracers that could potentially also play a role in urban aerosol formation (26). Their combined median daytime (11–16 h local time) emission flux was $6 \pm 1 \mu\text{g}/(\text{m}^2\cdot\text{h})$, exhibiting maximum 75 percentile fluxes up to $25 \mu\text{g}/(\text{m}^2\cdot\text{h})$ during morning hours.

To systematically investigate NMVOC flux patterns we used a nonnegative matrix factorization (NNMF) routine to investigate prominent urban NMVOC emission sources (*Methods*), where the normal chemical mass balance equations were applied to fluxes rather than concentrations. The usage of EC data has the advantage of eliminating covarying factors in such an analysis (e.g., changes in boundary-layer height or advection of nonlocal air masses) that typically limit the applicability of chemical mass balance models to complex urban NMVOC concentration datasets (*Methods*). Based on NMVOC tracers, typical tracer emission ratios, diurnal behavior, traffic activity, weekend–weekday variation, and temperature and wind-directional dependencies, we were able to identify nine important urban emission sources that represent four important emission categories: (i) cooking and roasting, (ii) traffic and combustion sources, (iii) biogenic emissions, and (iv) solvents. The corresponding source factor distributions are illustrated in Fig. 2 and detailed in Table S3. NMVOC emissions from

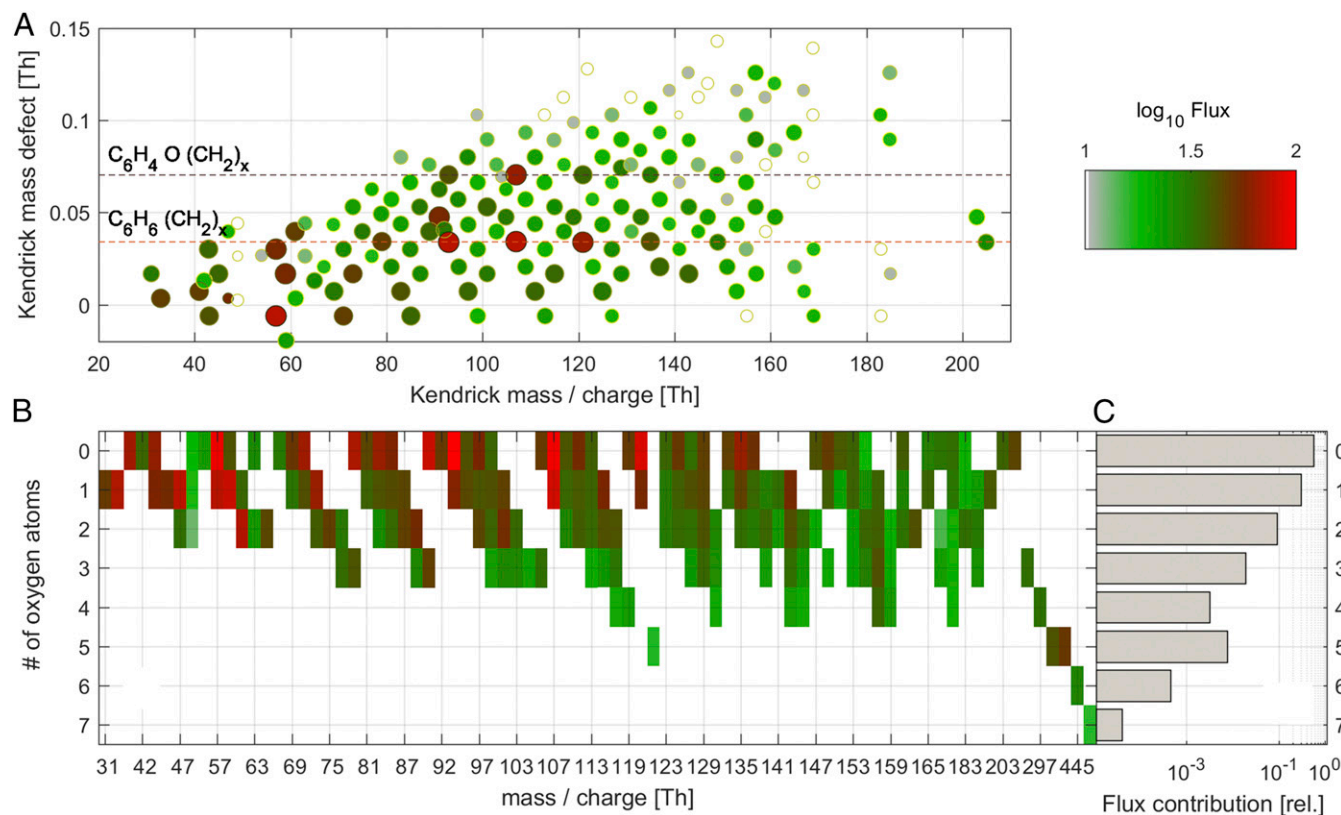


Fig. 1. Kendrick mass defect plot (A) in the lower molecular range. (B) Ions are binned according to nominal molecular weight and number of oxygen atoms. (C) The relative contribution to the median observed flux is depicted. To illustrate the interpretation of the mass defect plot we single out two cases (the benzene and benzaldehyde series), where all homologs for each compound lie on the indicated horizontal dashed lines. The color-bar scales with the logarithm of medium daytime fluxes is in units of nanomoles per square meter per second.

combustion sources were characterized by high loadings of aromatic compounds such as benzene and toluene which yielded a source factor ratio of 2.4 (i.e., toluene flux/benzene flux), which is typical for vehicular exhaust and evaporative/cold start emissions. Measurements of benzene fluxes have been conducted in a number of cities and observations reported here [$20 \pm 20 \mu\text{g}/(\text{m}^2\cdot\text{h})$ (24-h average)] are generally within the range [$14\text{--}140 \mu\text{g}/(\text{m}^2\cdot\text{h})$] observed in other European cities (Table S2). The cooking/frying factor was dominated by ions that can be associated with high loadings of a series of alkenals, which have recently been investigated by PTR in detail (27). Roasting/burning activities were characterized by typical marker species such as acetonitrile, dioxin, furan, 2- and 3- methylbutanals, and furfurals (28, 29). Solvents and health-care and skin products appeared in several separate source factors containing siloxanes and subsumed in the solvent category. In particular, source factors 6, 7, and 9 contained signatures of exogenous human emissions (e.g., siloxanes). Directly exhaled breath emissions would likely be collocated in these factors (30), which also contained typical NMVOC signatures from disinfectants and human emissions (i.e., lightweight alcohols and carbonyls). Another source factor (factor 8) is likely also partially associated with indoor air signatures involving the application of paints and solvents. This factor contributed $\sim 15\%$ of the overall OVOC emission flux during the entire campaign. The analysis was also able to extract two distinct biogenic source factors, one dominated by higher terpenes (i.e., mono- and sesquiterpenes), exhibiting a pronounced temperature dependence, and the other a light- and temperature-dominated factor, mostly comprised of isoprene and acetaldehyde. The NNMF analysis (Fig. 2) reveals a quite complex picture where many oxygenated species are associated with multiple urban sources.

How well can the overall volatile oxygenated NMVOC flux be constrained by PTR ionization? To answer this question we take advantage of the good separation of individual source profiles based on NNMF. While greatly reduced compared with electron impact ionization (31), fragmentation during PTR represents one limiting factor in the interpretation of mass spectra (32). The

reported OVOC fluxes therefore generally represent lower limits, primarily due to the leakage of oxygen during PTR ionization, particularly for alcohols (e.g., dehydration during charge transfer). In flow-drift tube experiments, such as PTR, fragmentation of NMVOC for low to moderate electric field strengths (e.g., $E/N < 110 \text{ Td}$) is primarily controlled by the ionization energy rather than the kinetic energy. A great wealth of studies for swarm-type experimental setups (33) exists, demonstrating that PTR leakage of oxygen due to fragmentation is typically (i.e., average of all measured compounds) on the order of $< 5\%$ for ketones, 15% for aldehydes, $< 5\%$ for ethers, $< 10\%$ for carboxylic acids, 30% for peroxides, 40% for diols, and 70% for alcohols. Fragmentation tends to be greatest for light- to intermediate-weight alcohols. It generally decreases with the size of a molecule because the number of internal degrees of freedom increases, which can efficiently distribute excess energy, thereby minimizing the probability of breakup. To gain more insight into the effect of fragmentation we conducted a sensitivity experiment taking advantage of results from the NNMF. Based on known or deduced fragmentation patterns we estimated the effect of oxygen leakage on the calculated bulk oxygen content of the observed NMVOC flux (Supporting Information). Fig. 3 summarizes results for the bulk flux of OVOCs. The shaded stacked area depicts measured OVOC fluxes grouped according to the number of oxygen atoms, where the dashed line represents an upper limit based on the sensitivity experiment on PTR fragmentation analysis. The bulk OVOC flux ratio (i.e., OVOC/NMVOC flux) lies between $46\text{--}66\%$ (best estimate: 56%), and the corresponding O/C content of the emitted NMVOC pool is bound between $18\text{--}35\%$ (best estimate: 27%). The fraction of OVOCs remains high with increasing molecular weight. This large abundance of oxygenates could exert an important influence on local OH reactivity.

How much of the observed upward OVOC flux can theoretically be explained by known photochemistry? A characteristic timescale (H/u^*) of atmosphere–surface exchange can be calculated from surface layer scaling theory, where u^* represents the friction velocity and H the measurement height of the sensor

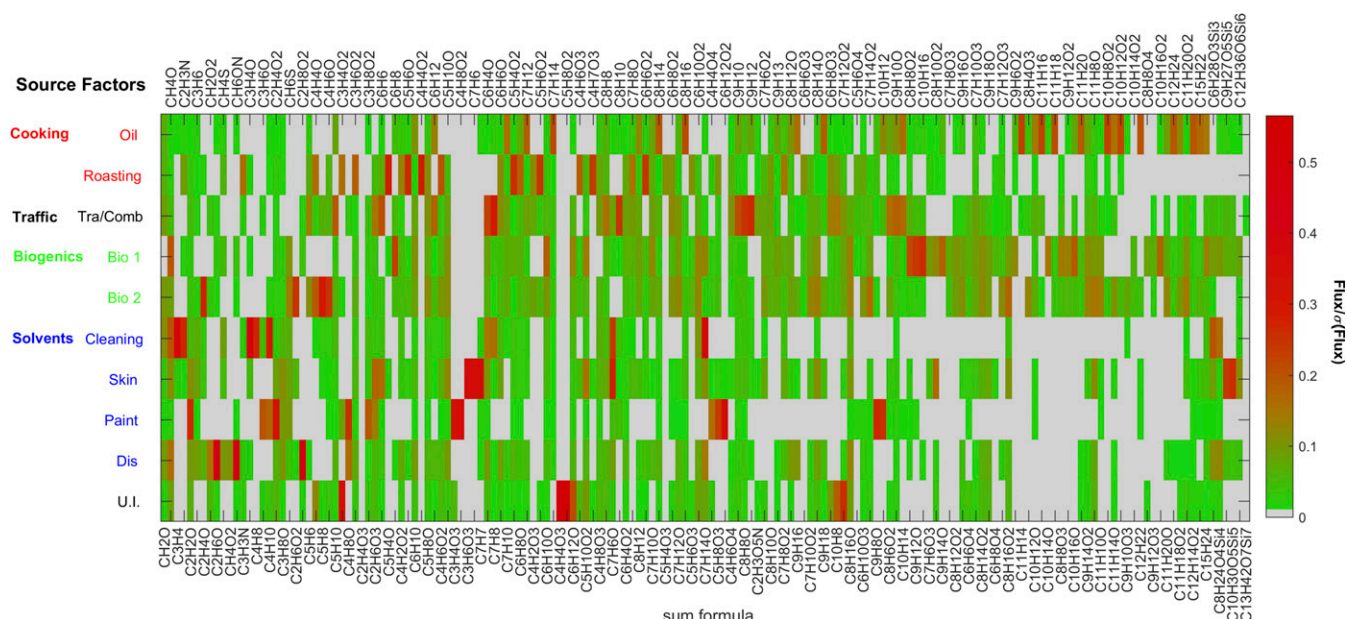


Fig. 2. NMVOC fingerprint from the NNMF analysis. The color code is proportional to the flux variability. Source factors are grouped as Cooking (Oil, oil frying; Roa, roasting and burning); Traffic (Tra/Comb, traffic and combustion sources); Biogenics [Bio1, biogenic VOCs 1 (temperature-dependent); Bio2, biogenic VOCs 2 (light- and temperature-dependent)]; Solvents (cleaning, cleaning agents/indoor air/detergents; Dis, disinfectants/indoor air; Paint, paint application/solvents; Skin, skin, human emissions/health-care products). U.I. is a factor that remains unidentified. The chemical composition is sequentially plotted in the Hill notation on both axes for better readability, starting in ascending order.

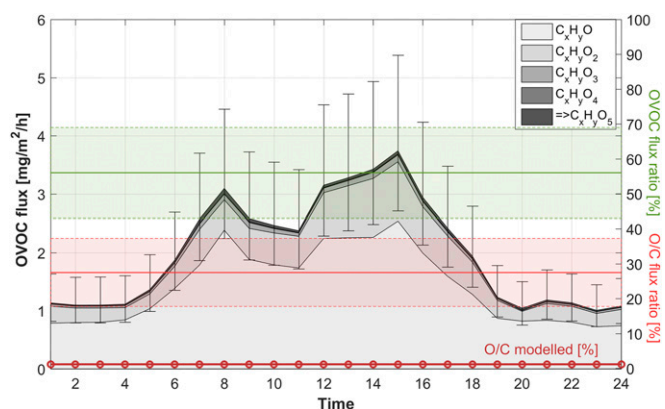


Fig. 3. Urban OVOC flux: Left axis: study average diurnal OVOC flux binned according to the isobaric oxygen content. Error bars represent upper and lower limits of the OVOC flux inferred from the uncertainty analysis. The red line represents the measured (24 h) mean O/C bulk flux ratio, and the green line is the measured (24 h) mean molar OVOC flux ratio (i.e., OVOC/NMVO). The shaded areas mark the combined uncertainty. The red dotted line illustrates the incrementally modeled O/C production ratio predicted after 600 s of photochemical processing. The anthropogenic OVOC flux was corrected to exclude influence of local biogenic emissions based on the factor analysis. Their inclusion would increase the O/C content by ~10%. The total NMVO flux was corrected for lightweight aliphatic compounds not detected by PTR based on urban enhancement ratios reported in the literature (ref. 34 and *Supporting Information*).

above the emission source injection height. For typical conditions at the present field site the turbulent timescale between emission and detection at the sensor is on the order of 30 s ($H/u^* = 15/0.5$). In a Lagrangian sense, transport times would certainly not exceed 600 s. To produce an equal amount of O/C content compared with the observed NMVO bulk flux (Fig. 3) it would take about 4 h of photochemical processing. This analysis therefore provides a second line of argument that the bulk of the released OVOC flux is likely associated with primary emission sources.

Discussion and Conclusion

Primary urban NMVO emission inventories are still considered quite uncertain (35) due to a lack of a quantitative understanding of characteristic bottom-up source emission profiles. In Europe the most comprehensive review is available through the GENEMIS project (35). Based on our data, the measured bulk urban OVOC flux would be at least about a factor of $2.1_{-0.4}^{+0.5}$ higher than projections used in these emission inventories (Table 1). Comparing to recommended values by the Intergovernmental Panel on Climate Change, we calculate a factor of $3.8_{-0.4}^{+0.5}$ higher contribution of primary emitted OVOCs. Rationing the total measured urban

NMVO flux to CO_2 , and comparing it to current state-of-the-art emission inventories indicates a three to four times higher urban NMVO flux. The measured NMVO/ CO_2 flux ratio during this study is $1.6\% (\pm 0.8\%)$ [gC/gC]; the corresponding NMVO/ CO_2 flux ratio is $3.6 (\pm 1.9)$ [gC/gC]. These ratios are three to four times higher than those inferred from anthropogenic emission inventories (Table 1) (35–40), which partition anthropogenic NMVO emissions such that about 50% is associated with road traffic and urban/residential source categories, which are a focus of this study. Uncertainty analysis (*Supporting Information*) suggests that measurements presented here likely lead to a lower estimate due to systematic errors in the analysis of OVOC. Comparison of typical urban NMVO flux ratios with other cities, where selected data are available (*Supporting Information* and Table S2), indicates that the results obtained for central Europe lie within 30% of other urban areas. Comparison with nonannex 1 countries is more uncertain due to the scarcity of data. When we investigate flux ratios relative to benzene, measurements conducted in Mexico City (18) indicate that toluene fluxes in nonannex 1 countries could be higher compared with European cities (i.e., by a factor of 1.9 in Mexico City). However, methanol fluxes in Mexico City were lower by 55% relative to benzene compared with European datasets. While nonannex 1 countries tend to have higher industrial emissions (41), our analysis focuses strictly on typical urban emission source categories, which comprise about 50% of the global total anthropogenic NMVO budget and exclude NMVO emitted from industrial activities. As mentioned, annex 1 countries have already mandated a gradual manufacturing shift toward oxygenated solvents, starting to replace aromatic-based solvents in household products and paints. In this context Asian emissions likely play an important role. While NMVO concentration measurements show significant variability across China (42, 43), reports (42) for acetone and acetaldehyde emission ratios in eastern China that were inferred indirectly based on enhancement ratios lie surprisingly close to the European flux emission ratio data reported in Table 1. For example, the acetone/benzene (acetaldehyde/benzene) enhancement ratio was reported to be 2.4 (3.2), comparable to the European average of 2.7 (3.3). Similar data were published for the United States (44), albeit we caution that these indirect estimation methods are subject to larger uncertainties than the direct flux measurements reported here. Currently there are no comprehensive NMVO flux data available to compare with across nonannex 1 countries, and NMVO flux measurements, particularly for Asia, would fill an important gap. We assume that the variability of important OVOC markers across different sites listed in Table S2 is a promising starting point to estimate the impact on global anthropogenic emissions. Based on the annual anthropogenic bottom-up NMVO flux from three global emission extrapolations, our results would yield a new adjusted anthropogenic NMVO emission flux of 330_{150}^{480} Tg/y assuming that global urban residential and road traffic emission scale with our

Table 1. Comparison of anthropogenic emission inventories with current measurements

Inventory	Annual NMVO flux, TgC/y	Ratio: urban/total	NMVO/ CO_2 , ^{*†} gC/gC	OVOC/NMVO, % w	Type	Source
ACCMIP [‡]	143	0.47	$4.4\text{e-}3^*$	N/A	Gridded	36
EDGAR [‡]	136	0.42	$4.1\text{e-}3^*$	N/A	Gridded	37
TAR [‡]	161	N/A	$1.0\text{e-}2^*$	14	Total budget	38
GENEMIS	N/A	N/A	N/A	27	European bottom-up	35
National	N/A	N/A	N/A	33	National bottom-up	39
COPERT	N/A	N/A	$3.7\text{e-}3$	10	Road transport bottom-up	40
EC	N/A	N/A	$1.6\text{e-}2 \pm (0.8\text{e-}2)$	56_{46}^{66}	Top-down flux measurements	This work

N/A, not assessed.

^{*}For inventories that do not explicitly report CO_2 the ratio was converted to the measured urban CO/CO_2 flux ratio measured here (4.1 ± 0.8 ppbv/ppmv).

[†]Values for gridded and source speciated inventories are based on urban-residential source categories (e.g., SNAP97: 2, 6, 7, 9).

[‡]Retrieved through the GAIA webportal: eccad.aeris-data.fr.

results. This is about twice what is currently included in most atmospheric chemistry and climate models (Table 1). Overall, measurements reported here and across annex 1 countries likely reflect a lower conservative estimate for upscaled global anthropogenic NMVOC emissions, because annex 1 countries are generally thought to have implemented stricter emission control standards than nonannex 1 countries over the past decades. Our measurements reveal that the contribution of OVOC to this budget is particularly uncertain, and that, aside from potential long-range transport from industrial sources (45), a number of individually small fluxes add up to a sizeable urban OVOC emission flux. This additional reactive carbon may have a significant influence on modeled SOA, atmospheric new particle formation, radical sources, and OH reactivity observed in urban environments.

Methods

Instrumentation. For NMVOC a PTR-QiTOF instrument (Ionicon) was operated in hydronium mode at standard conditions in the drift tube with an electric field strength (E/N) of 112 Townsend. The instrument included a quadrupole interface to increase sensitivity. For acetone, the instrument yielded a typical sensitivity of 1,550 Hz.ppbv⁻¹ (parts per billion by volume) with a flux detection limit (S/N = 3) of 70 μg/(m²·h) at a mass resolution (m/Δm) of about 3,700. Lowest detectable fluxes for individual 30-min averaging intervals observed on the ¹³C isotope of acetone were 2–4 μg/(m²·h). The inlet line was set up to sample ambient air from a turbulently purged 3/8-inch Teflon tube. The overall delay time through the 17-m-long inlet line was about 2 s. Every 7 h, zero calibrations were performed for 30 min providing VOC free air from a continuously purged catalytical converter through a setup of software-controlled solenoid valves. In addition, known quantities of a suite of VOC from a 1-ppm calibration gas standard (Apel & Riemer) were periodically added to the VOC-free air and dynamically diluted into low ppbv mixing ratios. Mixing ratios for compounds, where no calibration standards were available, were calculated based on standard operating procedures for PTR-TOF-MS analysis including humidity, duty cycle, and transmission corrections (46, 47). For CO₂ and H₂O a closed-path EC system (CPEC 200; short inlet, enclosed IRGA design; Campbell Scientific) measured 3D winds along with CO₂ and H₂O mixing ratios. An additional 3D sonic anemometer (CSAT3; Campbell Scientific) was available for turbulence measurements at an alternative height level. Calibration for CO₂ was performed once a day. CO measurements were available for a limited amount of time in August 2015. Ambient mole fractions of CO were measured with a quantum cascade laser spectrometer (CWQC-TILDAS-76-D; Aerodyne) with a 76-m path length optical cell at a wavenumber of ca. 2,190 cm⁻¹. The QCL was operated at a pressure of ca. 4 kPa using a built-in pressure controller and temperature of the optical bench and housing was controlled to 35 °C. Fitting of absorption spectra at 2 Hz, storing of calculated dry mole fractions, switching of zero/calibration valves, control of pressure lock, correction for band broadening, and other system controls were realized by TDLWintel software (Aerodyne) run on a personal computer synchronized in time with the system collecting the anemometer data using NTP software (Meinberg).

EC. The budget equation of a scalar is

$$\frac{\partial C}{\partial t} + \bar{u} \frac{\partial C}{\partial x} = S, \quad [2]$$

where C is the concentration, which can generally be decomposed into a mean and fluctuating part ($C = \bar{C} + c'$), $\bar{u} (=u, v, w)$ is the 3D wind vector corresponding to the coordinates $\bar{x} (=x, y, z)$, and S is the local net source or sink term.

Typical subsidence rates are on the order of 1 cm/s and small compared with convective velocity scales (w^*) of 1–2 m/s. We therefore ignore the mean vertical motion ($\langle w \rangle$). Following Taylor's hypothesis and decomposing \bar{u} into mean and turbulent parts, while assuming negligible horizontal turbulent parts, we arrive at

$$\frac{\partial C}{\partial t} + \langle \bar{u}_{x,y} \rangle \frac{\partial \bar{C}}{\partial \bar{x}_{x,y}} + \frac{\partial \langle w' \cdot c' \rangle}{\partial z} = S, \quad [3]$$

where the second term on the left-hand side represents horizontal advection and the third term on the left-hand side is the vertical flux divergence. For stationary conditions and neglecting horizontal advection the surface atmosphere flux is then defined as

$$F = \langle w' c' \rangle, \quad [4]$$

where w' represents the vertical fluctuation of wind speed and c' the concentration fluctuation. Brackets denote the averaging interval. The ensemble average used here is 30 min. EC fluxes were calculated as the covariance between the rotated vertical wind speed and the tracer mole fraction using routines described previously (ref. 48; <https://www.geos.ed.ac.uk/homes/jbm/micromet/EdiRe/>). Quality control was performed according to devised procedures described elsewhere (49). These included raw data despiking, applying a stationarity test and test on developed turbulent conditions (e.g., u^* filtering). Systematic errors due to high frequency losses were obtained from cospectral analysis and corrected (50). The damping timescales of the measurements were 0.2 s (CO₂), 0.1 s (CO), and 0.4 s (NMVOC).

By definition EC measurements represent a net flux at the atmosphere-surface interface. Over vegetated areas it has been shown that the deposition of NMVOC can be significant (23–25). Over the urban surface within the flux footprint investigated here we did not detect any significant net deposition fluxes. These findings confirm the assumption of deposition parameterizations, that the combined surface resistance over urban areas is generally large (51). Based on the Wesely scheme (e.g., ref. 52) we calculate a typical canopy resistance of 16,000 s/m for a compound with a Henry's law constant of 220 M/atm (e.g., methanol) and environmental conditions during this study. For methanol [median measured emission flux: 103 μg/(m²·h)] the deposition flux could therefore result in a <1% underestimation of the measured emission flux.

NNMF. NNMf or positive matrix factorization (PMF) is applied in chemical mass balance modeling when no a priori source factor distribution is known. Various implementations and constraints have been proposed in the literature and have most recently been implemented and discussed by Paatero and Hopke (52). A challenge of PMF applied to concentration datasets in ambient air is often caused by confounding factors (e.g., meteorology such as boundary layer dynamics and advection), which can lead to correlations that are spurious. As a consequence, these methods can often not attribute every factor to a single-source fingerprint and additional constraints in the analysis were introduced in the past (53). To improve the selectivity of NNMf for the analysis of NMVOC sources here we apply an NNMf algorithm to measured EC fluxes. NNMf proved a valuable approach because we observed positive net emission fluxes for all ions relevant to the analysis. We apply NNMf such that

$$\vec{F}_n = \vec{W} \times \vec{H} + \sigma, \quad [5]$$

where, \vec{F}_n is a (n-by-m) matrix consisting of measured NMVOC EC fluxes, which are apportioned into nonnegative factors \vec{W} (n-by-k) and \vec{H} (k-by-m). Flux data were preconditioned according to micrometeorological considerations (discussed above). In addition, all NMVOC fluxes were divided by their SD [$F_n = F/\sigma(F)$]; the NNMf routine was used as implemented in MATLAB 8.6.0.267246 (R2015b), with a maximum number of iterations of 100, number of replicates of 50 (i.e., 50 independent runs with random start guesses), and a termination tolerance on relative change in the elements of W and H of $\sigma < 1e-4$. The optimal number of factors used for the analysis was chosen according to statistical measures and chemical fingerprints and is outlined in *Supporting Information* (Figs. S2 and S3).

Master Chemical Mechanism Box Model Setup. The Master Chemical Mechanism (MCM) developed by the National Centre for Atmospheric Sciences at the University of Leeds summarizes the state-of-the-art knowledge on tropospheric chemistry. The chemical mechanistic information was taken from MCM v3.3.1 (54) via the website mcm.leeds.ac.uk/MCM and processed for further analysis in MATLAB (The MathWorks) using the box model version of CAFÉ (55). Photolysis rates were incorporated from measurements of shortwave radiation (56). Meteorological data (temperature and humidity) were taken from measurements. No dilution was added. The model was initialized with measured NMVOC concentrations. Species not detected by PTR-QiTOF (e.g., lightweight alkanes, such as ethane) were initialized relative to benzene, taking typical urban enhancement ratios (25). NO_x and ozone was constrained by measurements obtained from a nearby air-quality station. To perform the sensitivity analysis, all species were allowed to change their concentrations throughout the model run. Model runs were conducted as a nondiluting box. Time integration of the chemical rate equations was performed with constant midday photolysis rates and performed for up to 4 h. Individual model runs were conducted for 300, 600, 1,800, 3,600, 7,200, and 14,400 s. The O/C ratio of the evolving NMVOC pool

was calculated based on the MCM-supported chemical SMILES database. To investigate the potential influence of anthropogenic terpenes (57) and anthropogenic NMVOC that are currently not included in the mechanism (58) we performed sensitivity experiments by including or excluding reactive NMVOC. Scenarios of the evolution of modeled O/C ratios are shown in Fig. S4. The O/C content of model simulations performed with and without reactive terpenes differed by about 10%, suggesting that NMVOC with rate constants

significantly lower than $5 \times 10^{-11} \text{ cm}^3 \text{ per molecule per s}$ (e.g., glycols, glycol ethers, esters, or diols) would impact incrementally produced O/C ratios by less than 10% on timescales relevant for O/C flux ratios (i.e., 300–600 s).

ACKNOWLEDGMENTS. This work was supported by the EC Seventh Framework Program (Marie Curie Reintegration Program, "ALP-AIR," Grant 334084) and partly by Austrian National Science Fund Grants P26931 and P30600.

- Williams J (2004) Organic trace gases in the atmosphere: An overview. *Environ Chem* 3:125–136.
- Singh HB, et al. (1995) High concentrations and photochemical fate of oxygenated hydrocarbons in the global troposphere. *Nature* 378:50–54.
- Lu KD, et al. (2013) Missing OH source in a suburban environment near Beijing: Observed and modelled OH and HO₂ concentrations in summer 2006. *Atmos Chem Phys* 13:1057–1080.
- Odum JR, et al. (1996) Gas/particle partitioning and secondary organic aerosol yields. *Environ Sci Technol* 30:2580–2585.
- Jimenez JL, et al. (2009) Evolution of organic aerosols in the atmosphere. *Science* 326: 1525–1529.
- Schobesberger S, et al. (2013) Molecular understanding of atmospheric particle formation from sulfuric acid and large oxidized organic molecules. *Proc Natl Acad Sci USA* 110:17223–17228.
- Lewis AC, et al. (2000) A larger pool of ozone-forming carbon compounds in urban atmospheres. *Nature* 405:778–781.
- Lee-Taylor J, et al. (2001) Explicit modeling of organic chemistry and secondary organic aerosol partitioning for Mexico City and its outflow plume. *Atmos Chem Phys* 11:13219–13241.
- Sheehy PM, et al. (2010) Oxidative capacity of the Mexico City atmosphere—Part 2: A RO_x radical cycling perspective. *Atmos Chem Phys* 10:6993–7008.
- Stephens S, et al. (2008) Weekly patterns of Mexico City's surface concentrations of CO, NO_x, PM₁₀ and O₃ during 1986–2007. *Atmos Chem Phys* 8:5313–5323.
- Ehlers C, et al. (2015) Twenty years of ambient observations of nitrogen oxides and specified hydrocarbons in air masses dominated by traffic emissions in Germany. *Faraday Discuss* 189:407–437.
- Ryerson B, et al. (2003) Effect of petrochemical industrial emissions of reactive alkenes and NO_x on tropospheric ozone formation in Houston, Texas. *J Geophys Res* 108:4249.
- Derwent RG, et al. (1998) Photochemical ozone creation potentials for organic compounds in northwest Europe calculated with a master chemical mechanism. *Atmos Environ* 32:2429–2441.
- Dolgorouky C, et al. (2012) Total OH reactivity measurements in Paris during the 2010 MEGAPOLI winter campaign. *Atmos Chem Phys* 12:9593–9612.
- Hu L, et al. (2013) Emissions of C₆–C₈ aromatic compounds in the United States: Constraints from tall tower and aircraft measurements. *J Geophys Res* 120: 826–842.
- McDonald BC, Gentner DR, Goldstein AH, Harley RA (2013) Long-term trends in motor vehicle emissions in U.S. urban areas. *Environ Sci Technol* 47:10022–10031.
- Council of the European Union (1999) EU Directive 1999/13/EC: Reducing the emissions of volatile organic compounds (VOCs). Available at eur-lex.europa.eu/legal-content/EN/TXT/?uri=celex:31999L0013. Accessed October 1, 2017.
- Velasco E, et al. (2009) Eddy covariance flux measurements of pollutant gases in urban Mexico City. *Atmos Chem Phys* 9:7325–7342.
- Langford B, et al. (2010) Fluxes and concentrations of volatile organic compounds above central London, UK. *Atmos Chem Phys* 10:627–645.
- Warneke C, et al. (2007) Determination of urban volatile organic compound emission ratios and comparison with an emission database. *J Geophys Res* 112:D10S47.
- Mellouki A, Le Bras G, Sidebottom H (2003) Kinetics and mechanisms of the oxidation of oxygenated organic compounds in the gas phase. *Chem Rev* 103:5077–5096.
- Karl T, et al. (2001) Eddy covariance measurements of oxygenated volatile organic compound fluxes from crop harvesting using a redesigned proton-transfer-reaction mass spectrometer. *J Geophys Res* 106:24157–24167.
- Park JH, et al. (2013) Active atmosphere-ecosystem exchange of the vast majority of detected volatile organic compounds. *Science* 341:643–647.
- Karl T, et al. (2010) Efficient atmospheric cleansing of oxidized organic trace gases by vegetation. *Science* 330:816–819.
- Nguyen TB, et al. (2015) Rapid deposition of oxidized biogenic compounds to a temperate forest. *Proc Natl Acad Sci USA* 112:E392–E401.
- Wu Y, Johnston MV (2017) Aerosol formation from OH oxidation of the volatile cyclic methyl siloxane (cVMS) Decamethylcyclopentasiloxane. *Environ Sci Technol* 51: 4445–4451.
- Klein F, et al. (2016) Characterization of gas-phase organics using proton transfer reaction time-of-flight mass spectrometry: Cooking emissions. *Environ Sci Technol* 50: 1243–1250.
- Gloess A, et al. (2016) Evidence of different flavor formation dynamics by roasting coffee from different origins: On-line analysis with PTR-TOF-MS. *Int J Mass Spectrom* 365:324–337.
- Coggon MM, et al. (2016) Emissions of nitrogen-containing organic compounds from the burning of herbaceous and arboraceous biomass: Fuel composition dependence and the variability of commonly used nitrile tracers. *Geophys Res Lett* 43:9903–9912.
- Stöner C, Edtbauer A, Williams J (2017) Real-world volatile organic compound emission rates from seated adults and children for use in indoor air studies. *Indoor Air* 28:164–172.
- Lindinger W, et al. (1998) Proton-transfer-reaction mass spectrometry (PTR-MS): On-line monitoring of volatile organic compounds at pptv levels. *Chem Soc Rev* 27: 347–375.
- de Gouw J, Warneke C (2007) Measurements of volatile organic compounds in the earth's atmosphere using proton-transfer-reaction mass spectrometry. *Mass Spectrom Rev* 26:223–257.
- Spanel P, Smith D (2013) On the features, successes and challenges of selected ion flow tube mass spectrometry. *Eur J Mass Spectrom (Chichester)* 19:225–246.
- Borbon A, et al. (2013) Emission ratios of anthropogenic volatile organic compounds in northern mid latitude megacities: Observations versus emission inventories in Los Angeles and Paris. *J Geophys Res* 118:2041–2057.
- Theloke J, Friedrich R (2007) Compilation of a database on the composition of anthropogenic VOC emissions for atmospheric modeling in Europe. *Atmos Environ* 41: 4148–4160.
- Lamarque JF, et al. (2010) Historical (1850–2000) gridded anthropogenic and biomass burning emissions of reactive gases and aerosols: Methodology and application. *Atmos Chem Phys* 10:7017–7039.
- Huang G, et al. (2017) Speciation of anthropogenic emissions of non-methane volatile organic compounds: A global gridded data set for 1970–2012. *Atmos Chem Phys Phys* 17:7683–7701.
- Ehhalt D, Prather M (2001) Atmospheric chemistry and greenhouse gases, 3rd Assessment Report, Chap 4 (Intergovernmental Panel on Climate Change, Geneva). Available at <https://www.ipcc.ch/ipccreports/tar/wg1/index.htm>. Accessed October 1, 2017.
- Loibl W, Orthofer R, Winiwarter W (1993) Spatially disaggregated emission inventory for anthropogenic NMVOC in Austria. *Atmos Environ* 16:2575–2590.
- Papadimitriou G, et al. (2013) TRACCs—Transport data collection supporting the quantitative analysis of measures relating to transport and climate change. Technical report EMISIA No. 13.RE.025.V1 (EMISIA SA, Thessaloniki, Greece).
- von Schneidmesser E, Monks PS, Plass-Duelmer C (2010) Global comparison of VOC and CO observations in urban areas. *Atmos Environ* 44:5053–5064.
- Yuan B, et al. (2013) VOC emissions, evolutions and contributions to SOA formation at a receptor site in eastern China. *Atmos Chem Phys* 13:8815–8832.
- Liu Y, et al. (2008) Source profiles of volatile organic compounds (VOCs) measured in China: Part I. *Atmos Environ* 42:6247–6260.
- de Gouw JA, et al. (2005) Budget of organic carbon in a polluted atmosphere: Results from the New England Air Quality Study in 2002. *J Geophys Res Atmos* 110:D16305.
- Gros V, et al. (2011) Volatile organic compounds sources in Paris in spring 2007. Part I: Qualitative analysis. *Environ Chem* 8:74–90.
- Graus M, Müller M, Hansel A (2010) High resolution PTR-TOF: Quantification and formula confirmation of VOC in real time. *J Am Soc Mass Spectrom* 21:1037–1044.
- Cappellin L, et al. (2012) On quantitative determination of volatile organic compound concentrations using proton transfer reaction time-of-flight mass spectrometry. *Environ Sci Technol* 46:2283–2290.
- Karl T, et al. (2002) Virtual disjunct eddy covariance measurements of organic compound fluxes from a subalpine forest using proton transfer reaction mass spectrometry. *Atmos Chem Phys* 2:279–291.
- Foken T, Leuning R, Oncley SP, Mauder M, Aubinet M (2010) Corrections and data quality. *Eddy Covariance: A Practical Guide to Measurement and Data Analysis* (Kluwer, Dordrecht, The Netherlands), 1st Ed, pp 85–131.
- Massmann W, Clement R (2010) Uncertainty in eddy covariance flux estimates resulting from spectral attenuation. *A Practical Guide to Measurement and Data Analysis* (Kluwer, Dordrecht, The Netherlands), 1st Ed, pp 67–96.
- Zhang L, Moran MD, Makar PA, Brook JR, Gong S (2002) Modelling gaseous dry deposition in AURAMS: A unified regional air-quality modelling system. *Atmos Environ* 36:537–560.
- Paatero P, Hopke PK (2009) Rotational tools for factor analytic models. *J Chemometr* 23:91–100.
- Zhao W, Hopke PK, Karl T (2004) Source identification of volatile organic compounds in Houston, Texas. *Environ Sci Technol* 38:1338–1347.
- Jenkin ME, Saunders SM, Pilling MJ (1997) The tropospheric degradation of volatile organic compounds: A protocol for mechanism development. *Atmos Environ* 31: 81–104.
- Wolfe G, Thornton J (2011) The chemistry of atmosphere-forest exchange (CAFÉ) model—Part 1: Model description and characterization. *Atmos Chem Phys* 11:77–101.
- Trebs I, et al. (2009) Relationship between the NO₂ photolysis frequency and the solar global irradiance. *Atmos Meas Tech* 2:725–739.
- Derwent RG, Jenkin ME, Passant NR, Pilling MJ (2007) Photochemical ozone creation potentials (POCPs) for different emission sources of organic compounds under European conditions estimated with a Master Chemical Mechanism. *Atmos Environ* 41: 2570–2579.
- Shin HM, McKone TE, Bennett DH (2015) Contribution of low vapor pressure-volatile organic compounds (LVP-VOCs) from consumer products to ozone formation in urban atmospheres. *Atmos Environ* 108:98–106.